

Long Lived Geomagnetic Storms and Coronal Mass Ejections

H. Xie^{1,2}, N. Gopalswamy², P.K. Manoharan³,

A. Lara⁴, S. Yashiro^{1,2}, and S. Lepri⁵

¹The Catholic University of America.

²NASA/GSFC.

³National Center for Radio Astronomy, Ooty, INDIA.

⁴Instituto de Geofisica, UNAM, Mexico

⁵University of Michigan

Abstract. Coronal mass ejections (CMEs) are major solar events that are known to cause large geomagnetic storms ($Dst < -100$ nT). Isolated geomagnetic storms typically have a main phase of 3 -12 hours and a recovery phase of around 1 day. However, there are some storms with main and recovery phases exceeding ~ 3 days. We trace the origin of these long-lived geomagnetic storms (LLGMS) to front-side halo CMEs. We studied 37 LLGMS events with $Dst < -100$ nT and the associated CMEs which occurred during 1998-2002. It is found that LLGMS events are caused by: 1) successive CMEs, accounting for ~ 64.9 % (24 of 37); 2) single CMEs, accounting for ~ 21.6 % (8 of 37); and 3) High speed streams (HSS) in corotating interaction regions (CIRs) with no related CME, accounting for ~ 13.5 % (5 of 37). The long duration of the LLGMS events was found to be due to successive CMEs and HSS events; the high intensity of the LLGMS events was related to the interaction of CMEs with other CMEs and HSS events. We find that the duration of LLGMS is well correlated to the number of participating CMEs (correlation coefficient $r = 0.78$). We also find that the intensity of LLGMS has a good correlation with the degree of interaction (the number of CMEs interacting with a HSS event or with themselves) ($r = 0.67$). The role of preconditioning in LLGMS

events, where the Dst development occurred in multiple steps in the main and recovery phases, has been investigated. It is found that preconditioning does not affect the main phase of the LLGMS events, while it plays an important role during the recovery phase of the LLGMS events.

1. Introduction

Intense geomagnetic storms generally occur when solar wind with intense, long-duration southward interplanetary magnetic field (IMF) impacts Earth's magnetosphere. During geomagnetic storms, southward IMF reconnects with Earth's geomagnetic field at the dayside magnetopause, resulting in a chain of events leading to the dramatic increase of the ring current westward, which induces a magnetic field opposite to the geomagnetic field and causes global depression in the horizontal component (H) of the geomagnetic field. It has been known since the work of Burton et al. [1975] that the intensity of geomagnetic storms is proportional to the interplanetary dawn-dusk electric field $E = -V_{sw} \times B_s / c$, where V_{sw} is the solar wind flow speed and B_s is the southward component of the IMF [e.g., *Tsurutani and Gonzalez, 1997; Gonzalez et al., 1994*]. Burton et al. [1975] provided a simple formula describing the dependence of the energy injection into the ring current system as a function of the solar wind electric field E , indicating that the duskward E is generally associated with the observed negative Dst peak (an index proportional to the kinetic energy of the ring current particles) during the storm. Using an empirical model, O'Brien and McPherron [2000] found that this energy injection is proportional to $E - E_c$, where the threshold to the electric field $E_c = 0.49 \text{ mV/m}$. Large-intensity storms are expected to be a more direct response to the interplanetary conditions, where their long life is mainly from the large value reached by $|\text{Dst}|$.

The Dst (disturbance storm time) index is based on the H-component of the geomagnetic field averaged over four near-equatorial observatories. The strength of geomagnetic storms can be measured by the Dst index. In the case of an isolated magnetic storm, the Dst decreases drastically in the main phase and then recovers gradually to its quiet time level in the recovery phase. An isolated magnetic storm normally lasts for 1 day with a typical main phase of 3 - 12 hours and a recovery phase lasting $\sim 14 \pm 4$ hours [e.g., *Dasso et al.*, 2002; *Tsurutani and Gonzalez*, 1997]. However, there are some geomagnetic storms, which have more complex structure and show multiple-step decreases in Dst in the main phase and/or recovery phases. These geomagnetic storms often have longer duration and higher intensity. We refer to geomagnetic storms with total duration exceeding 3 days as long-lived geomagnetic storms (LLGMS).

It is now well established that Coronal Mass ejections (CMEs) are the major causes for large geomagnetic storms ($Dst < -100$ nT) [*Bruechner et al.*, 1998; *Cane et al.*, 2000; *Gopalswamy et al.*, 2000, 2005; *Wang et al.*, 2002; *Webb et al.*, 2000; *Zhang et al.*, 2003]. High-speed streams (HSS) in corotating interaction regions (CIRs) cause only moderate to weak storms ($-100\text{nT} < Dst < -50$ nT). CMEs on the Sun are intrinsically magnetic entities with large fields; they also compress any IMF at their leading regions when they travel through the interplanetary (IP) medium and interact with other IP CMEs (ICMEs) and/or the ambient solar wind driving IP shocks. Manoharan et al. [2004] studied the influence of CME interaction on propagation of IP shocks, and found that the CME interaction tends to slow the shock. Southward magnetic field (B_s) in shock sheaths and ICMEs or magnetic clouds (MCs) contribute to the generation of the geomagnetic storms. Burlaga et al. [2001] studied a set of fast ejecta observed at 1 AU from February 5, 1998 to November 29, 1999 and found all MC

events and two complex ejecta resulting from the interaction of multiple CMEs, produced geomagnetic storms. When HSS encounter and interact with CMEs, they can further compress B_z and enhance geoeffectiveness [e.g., *Burlaga et al.*, 1987; *Burlaga*, 1995; *Gopalswamy et al.*, 2005].

Severe LLGMS events are often associated with complex interplanetary interaction regions [e.g., *Burlaga et al.*, 1987; *Cane and Richardson*, 1997; *Crooker et al.*, 1998, *Burlaga et al.*, 2002, 2003]. The common feature of the interaction regions is that they have relatively high and complex magnetic fields, which may consist of two or more B_s structures and cause a multi-step Dst decrease. Such a storm is the so-called multistep storm [*Tsurutani and Gonzalez*, 1997, *Kamide et al.*, 1998, *Gonzalez et al.*, 2001]. In general, multi-step storms result from consecutive impacts of southward B_s in different regions on the magnetosphere. Kamide (1998) performed a statistical analysis of more than 1200 geomagnetic storms for the period from 1957 –1991 and found that geomagnetic storms with two-step intensifications last longer and have larger storm size than the single-step storms. Grande et al. [1996] studied the March 23, 1991 two-step magnetic storm, and found that the first event was dominated by Fe^{+9} while the second by Fe^{+16} . The possible explanation for this is that the first event was caused by the B_s in the shocked sheath region, while the second was caused by the intrinsic fields in the MC since high charge states are associated with ICMEs [*Fenimore*, 1980; *Henke et al.*, 1998; *Gloeckler et al.*, 1999, *Lepri et al.*, 2001]. Gonzalez et al. [2001] showed that for some events the main phase might develop in more than two consecutive steps; these storms exhibit a slowly developed long-duration main phase and relate to complex southward B_s structure.

Kamide et al. [1998] argued that the two-step storm may result from the superposition of two successive modest storms. However, this assumption might be over simplified. More

studies indicate that the multi-step storms could not be the result of simple superposition of individual ring current developments [e.g., *Chen et al.*, 2000; *Kozyra et al.*, 1998, 2002]. *Chen et al.* [2000] demonstrated that two intervals of enhanced convection are not inherently more effective at producing a strong ring current than one longer interval. *Kozyra et al.* [1998] showed that the inner magnetosphere retains little or no memory of previous injections since earlier injections are swept out of the dayside magnetopause as new population for the plasma sheet moves into the inner magnetosphere. The authors suggested that preconditioning occurs in a multi-step storm through the cumulative effects of the successive storms on the plasma sheet population [*Kozyra et al.*, 1998, 2002]. Another possibility is that previous storms prime the inner magnetosphere through the substorm-associated accumulation of O^+ ions injected from the ionosphere during intense storms [*Hamilton et al.*, 1988; *Daglis*, 1997].

In this paper, we conduct a statistical study of LLGMS, successive CMEs, and interaction regions of complex ejecta, IP shocks, and HSS to investigate their effects on the duration and intensity of these storms. We identified 37 LLGMS events with $Dst < -100$ nT during 1998-2002. We studied the storm duration, storm intensity, IP driver of the storm, and the cause of associated B_s structures. We found that when the driver of the LLGMS is associated with multiple CMEs (64.9% of the cases), the duration of LLGMS events is well correlated with the number of participating CMEs in an LLGMS and the intensity of LLGMS has a good correlation with the degree of interaction (the number of CMEs interacting with a HSS event or with themselves, see definition in Section 3). Also, we investigated the role of cumulative preconditioning from consecutive storms in the multi-step ring current intensifications in LLGMS events.

2. Methodology

We used the Dst index data from the World Data Center in Kyoto (<http://swdcwww.kugi.kyoto-u.ac.jp/dstdir/>) to identify the geomagnetic storms. The associated CMEs observed by the Solar and Heliospheric Observatory (SOHO) mission's coronagraphs were obtained from the CME catalog (http://cdaw.gsfc.nasa.gov/CME_list) (Yashiro *et al.*, 2004). The solar source regions of the CME were identified from the on-line Solar Geophysical Data (SGD) as the location of the associated GOES *X-ray* flares in order to see if CMEs were front-side and traveling toward Earth. When GOES *X-ray* flare information was not available, we used movies from the Extreme-ultraviolet Imaging Telescope (EIT) on board SOHO and Yokohoh mission's soft X-ray telescope to identify the location of the eruption. In order to identify the ICMEs, we use Fe charge state data from Advanced Composition Explorer/ Solar Wind Ion Composition Spectrometer (ACE/SWICS), the solar wind plasma density, temperature, and flow speed from the Solar Wind Experiment (SWE) aboard the Wind spacecraft; and the magnitude $|B|$ and the B_z component of the interplanetary magnetic field from Wind Magnetic Field Investigation (MFI). Also, we used the IP shocks from Wind online shock list (http://pwg.gsfc.nasa.gov/wind/current_listIPS.htm), the MC list from *Lepping* [2005], the MC-like (MCL) structures from Wind MFI online list (<http://lepmfi.gsfc.nasa.gov/mfi/MCL1.html>), and the CME trajectories obtained from empirical CME arrival (ECA) model [Gopalswamy *et al.*, 2000, 2001] to identify the arrival of successive CMEs at 1 AU.

The ECA model is based on the empirical interplanetary acceleration of CME, which was found to be

$$\begin{aligned} a &= 2.193 - 0.0054u_0 \quad (s < d_1) \\ a &= 0 \quad (s > d_1) \end{aligned} \quad (1)$$

where a is acceleration in units of $[\text{ms}^{-2}]$, and u_0 is initial CME speed in units of $[\text{kms}^{-1}]$,

s is the heliocentric distance along the line of sight, d_1 is the acceleration ceasing distance. The ECA model assumed that the acceleration ceases at a distance d_1 in interplanetary space when the CME speed is the same as the ambient solar wind speed. Assuming $d_2 = 1\text{AU} - d_1$, the CME travel time is computed as the sum of time t_1 to travel d_1 and t_2 to d_2 : $t = t_1 + t_2$, where

$$t_1 = \frac{-u + \sqrt{u^2 + 2ad_1}}{a}, \quad t_2 = \frac{d_2}{\sqrt{u^2 + 2ad_2}}. \quad (2)$$

The CME trajectories can be obtained from the basic kinematic equations:

$$\begin{aligned} s &= u_0 t + at^2 / 2 & (t < t_1) \\ s &= u_1 t + d_1 & (t > t_1) \end{aligned} \quad (3)$$

The ECA model requires the initial radial speed of a CME as input parameter. One of the difficulties in obtaining the CME initial speed is the uncertainty due to projection effects. Even though Earth-impacting CMEs typically originate from close to the Sun center [Gopalswamy *et al.*, 2000], there is no easy way to determine whether a halo or partial halo CME would reach Earth. In this work, we attempt to correct for the projection effect and resolve the criterion for a CME to reach Earth by an improved CME cone model (Xie *et al.*, 2004). In the cone model, the orientation of a CME is defined by the longitude angle α (or ϕ) and the latitude angle θ (or λ); the angular width of the CME is defined by 2ω , as shown in Figure 1. The actual radial speed of the CME is given by:

$$\begin{aligned}
V_r &= \frac{dr}{dt} = \frac{V_{x_c'}}{\cos \omega \cos \theta - \sin \omega \sin \theta \sin \delta}, \\
\text{or} \\
V_r &= \frac{dr}{dt} = \frac{V_{y_c'}}{\sin \omega \cos \delta},
\end{aligned} \tag{4}$$

where $V_{x_c'}$ and $V_{y_c'}$ are the components of the CME projection speed along x_c' and y_c' axes in the plane of the sky (POS), respectively, δ is the azimuthal angle defined as $\delta = \tan^{-1}(z_c/y_c)$ in the cone coordinate. The projection speed V_r on POS along the position angle (PA) is related to $V_{x_c'}$ and $V_{y_c'}$ as follows: $V_{x_c'} = V_r \sin(\alpha - PA)$ and $V_{y_c'} = V_r \cos(\alpha - PA)$.

The criterion for a CME to arrive at Earth is given by

$$\omega \geq \beta + \Delta, \tag{5}$$

where β is the angle between the cone central axis and the line-of-sight (LOS), L is the displacement of the CME source region to LOS, and Δ is the angle between the LOS and one (Earthward) of the cone lateral projections, $\Delta=L/1AU$ (see Figure 2) [Xie *et al.*, 2004].

3. Data

Table 1 lists the 37 LLGMS events. In the table, the Dst minimum (Dst_{min}) time, Dst_{min} value, storm onset time, storm end time, storm duration, IP driver, CME first appearance time in C2, associated solar source location, storm category and comments are listed. The storm onset time is defined by the occurrence time of storm sudden commencement (SSC), which is caused by an intensification of the magnetopause current as the enhanced solar wind dynamic pressure (due to the IP shock) drives the magnetopause inward. The SSC is normally associated with the occurrence of IP shocks, but may not be recognizable when the geomagnetic field is already depressed (preconditioning). When there is no clear identification of an SSC, we define the storm onset time as the time when Dst starts decreasing. The storm

end time is defined by the time when the Dst recovers to $Dst_0(1/e)$, where Dst_0 is $-50 nT$, the minimum intensity of modest storms. The LLGMS events are classified as 1) Multiple CME (M) type, 2) Single CME (S) type, and 3) CIR (C) type. In column 10, the first number in parentheses represents the number of participating CMEs in an LLGMS. The criterion to determine the number of participating CMEs in the LLGMS is to examine whether the arrival time of CMEs from the ECA model falls into the interval of LLGMS plus an error of ± 21.4 hours, i.e, two times of root-mean-square (rms) of ECA model, where the average prediction error (rms) was estimated as 10.7 hours [Gopalswamy *et al.*, 2001]. The second number in column 10 represents the degree of interaction, which is defined as follows: if the interaction occurs between a CME and a HSS, the interaction is of degree 1, otherwise, the degree is equal to the number of CMEs involved in the possible interaction. We applied criterion (5) to identify if a CME has a component heading toward Earth [Xie *et al.*, 2004] and extrapolated the CME trajectories from the Sun to 1 AU (see bottom panel of Figure 3). If the trajectories of two CMEs intersect, then it indicates that an interaction has occurred between the two CMEs (the distance where the CME interaction occurs is indicated in the y-axis of the CME height-time plot). The third letter 'h' in parentheses of column 10 denotes cases involving an HSS event.

Figures 3 - 6 present four examples of LLGMS events, in which we show the associated Dst variation and related solar wind parameters. Figure 3a shows the Dst index, Fe charge state data $\langle Q_{Fe} \rangle$, $|\mathbf{B}|$ and B_z , solar wind density N , temperature T , flow velocity V , and the trajectories (height-time profiles) of the associated CMEs for the 2000 February 12 event. In this event the LLGMS lasted for ~ 4.9 days (February 11 - 16). There were two dips (dip 'A' and dip 'B') in the main phase and two dips (dip 'C' and dip 'D') in the recovery phase

(see arrows in the Dst plot). Four CMEs (labeled with numbers on the CME trajectories of Figure 3a) have been found to be associated with this event. Three forward fast shocks F_1 (on February 11 at 02:33 UT related to CME 1), F_2 (on Feb. 11 at 23:38 UT resulting from the possible interaction of CME 2 and CME 3), and F_3 (on Feb. 14 at 07:18 UT corresponding to CME 4), were present in this event. CME 2 and CME 3 arrived at about the same time at ~ 1 AU. It is likely that CME 3 has caught up with CME 2 and the two CMEs merged resulting in a single complex ejecta (ICME 2). A MC (February 12, 17:06 - February 13, 00:36) with a complex leading sheath region formed part of ICME 2. An anomalous high Fe charge state interval in the event corresponds to with this complex ICME 2. Figure 3a shows that the ICME 2 has run into the rear part of ICME 1, causing compressed B_s in the trailing region of ICME 1. Possible interaction occurred between CME 1, CME 2 and CME 3. Dip 'A' in the main phase was caused by the compressed B_s in the rear part of ICME 1. Dip 'B' followed by a small dip was produced by the B_s structures in the sheath region and the MC, respectively. The MC was followed by a HSS-like structure with high T and low N , causing Dip 'C' in the recovery phase, where the Dst value was nearly constant for more than 10 hours. However, this HSS-like structure could also likely be the extension of the ICME 2 since no apparent coronal hole was observed at low latitude near the sun disk (ICME interval is typically featured with low T and reduced field fluctuations, but such features may not be present in some ICMEs [*Cane et al.*, 2003]). CME 1, CME 3, and CME 4 originated from the active region AR8858 when it was at N25E26, N31E04, and N26W26 as the Sun rotated westward. CME 2 originated from AR8853 at S17W40. Figure 3b shows the LASCO images of the four successive CMEs associated with this event, superposed with EIT images.

Figure 4 shows the Dst index, $\langle Q_{Fe} \rangle$, $|\mathbf{B}|$, B_z , N , T , V , the trajectories of the associated CMEs and CME C2 images for the 2002 April 20 event. In this event the LLGMS extended from April 17 to April 23 and the storm lasted for ~ 5.7 days. The LLGMS consists of two consecutive storms, which are associated with two successive MCs: MC 1 (April 18, 04:18 – April 19, 02:18) and MC 2 (April 20, 11:48 – April 21, 16:48). Two forward shocks F_1 (April 17 at 11:01 UT), F_2 (April 19 at 22:22 UT), and one reverse shock R_2 (April 20 at 04:40 UT) were found ahead of the MC 1 and MC 2, respectively. The MC 1 produced a typical two-step ring current intensification, i.e., dip ‘A’ and dip ‘B’ in the Dst plot of Figure 4, caused by the B_s in the sheath region and the cloud, respectively. This two-step feature was not seen in the second storm; only dip ‘D’ was produced by the B_s in the sheath region of shock F_2 . The solar origin of Dip ‘C’ was difficult to define since we did not find any reported CME on the Sun. It might be either due to a short HSS-like structure or an ejecta associated with a missing CME. Two CMEs, which caused the two MCs, respectively, were observed to be associated with this event. CME 1 originated from active region AR9905 at S15W01 with an M1.2 flare and CME 2 originated from active region AR 9906 at S14W34 with an M2.6 flare. Fe charge state data showed two clear anomalous stages for this event, and their onsets are in near coincidence with the leading edge of the MCs. Figure 4b shows LASCO C2 images of CME 1 and CME 2.

Figure 5 shows the Dst index, $\langle Q_{Fe} \rangle$, $|\mathbf{B}|$, B_z , N , T , V , and the trajectory of the associated CME for the 2000 April 07 event. The LLGMS lasted 5.8 days, extending from 2000 April 06 to 2000 April 12 [Gopalswamy, 2002]. A fast forward shock F_1 on April 06 at 16:27 UT and a reverse shock R_1 on April 07 at 09:16 UT, were present in this event. The Dst minimum of the LLGMS is ~ -288 nT, which was caused by the B_s in the sheath region of F_1 . A HSS-like structure has caused the long recovery phase of the LLGMS. Shock F_1 was

associated with a fast halo CME with actual speed of 1139 km/s and actual angular width of 128° obtained by the cone model.

Figure 6 shows the corresponding data for the LLGMS from 2002 October 06 to 2002 October 13. The LLGMS had lasted for ~ 6.9 days with modest intensity of the minimum Dst ~ -115 nT. It was produced by a HSS emanating from a low-latitude coronal hole, which was present a few days earlier near the disk center at 22:00 UT on the 2002 October 05 EIT image.

4. Statistical Results

4.1 Associations

First of all we find that the LLGMS events were produced by complex B_s structures in various interaction regions: 1) IP shocks and complex ICMEs related to successive CMEs,; 2) single IP shock and ICME (MC); 3) HSS events in CIRs. Note that both type 1) and type 2) might be mixing with possible HSS events. Of the 37 LLGMS events, 24 (64.9%) were associated with multiple CMEs, 8 (21.6%) were caused by single CMEs, and 5 (13.5%) were related to CIRs with no CME involvement.

4.2 LLGMS Properties

4.2.1 LLGMS Duration

In order to study the relationship between the duration of LLGMS and successive CMEs and their interaction with HSS events, the LLGMS events were divided into the following six groups: (a) all multiple CME cases; (b) all single CME cases; (c) all CIR cases with no related CME; (d) Multiple CME cases with ≥ 3 CMEs; (e) all cases involving HSS; (f) cases with no HSS and ≤ 2 CMEs. Note, that the classification of the groups (a-b-c-d-e-f) does not imply disjoint sets, e.g., in this case group (d) is a subset of group (a). We use group (d) to

study the effects of multiple CMEs (≥ 3) on the duration (Dur) of LLGMS, and group (e) to study the effects of HSS events on Dur . Group (f) is used to study the cases without either multiple CMEs or HSS. Figure 7 presents the distribution of the duration of LLGMS for six different groups. The median durations for the above six groups are 4.1, 4.6, 6.9, 5.4, 5.8, and 3.4 days, respectively. In the multiple CME group, the LLGMS events were associated with more than one B_s structure and the Dst developed in multiple consecutive steps, causing the long duration. The median durations for the multiple CME type (a) and (d) are 4.1 and 5.4 days, respectively. The median duration for the CIR group is the longest with a median value of 6.9 days. The second longest duration is for all the LLGMS events involving HSS. The nature of the duration in the events involving HSS is due to the long periods of B_s fluctuations within HSS. As expected, the median duration for group (f) with no HSS and ≤ 2 CME is the shortest among the six groups, with a median value of 3.5 days. Therefore, the CIRs and HSS are associated with the largest duration LLGMS events. If an LLGMS is associated with successive CMEs, the duration of the storm increases with the number of the participating CMEs. Figure 9a shows the relationship between the LLGMS duration and the number (nc) of participating CMEs. We find that there is a good correlation between the duration and nc with correlation coefficient (r) of 0.78.

Note that some single CMEs (with no HSS) events can reach long durations (~ 3 days) because of the very large storm intensity in these events, which caused relatively long recovery phase of the storms.

4.2.2 LLGMS Intensity

To study the effect of the interaction CMEs with other CMEs and HSS on the intensity of LLGMS, we group the LLGMS events as in subsection 4.2.1, except that group (f) is

classified as cases with no CME interaction. We extrapolated the CME trajectories from the Sun to 1 AU (see bottom panel in Figure 3) to decide if two CMEs interact, and applied criterion (5) to identify if a CME would reach Earth [Xie *et al.*, 2004]. Figure 8 presents the histogram of the Dst_{min} of LLGMS of the above groups. The median values of Dst_{min} for the six groups are -157, -155, -115, -181, -133, and -116 nT, respectively. The multiple CME groups possessed relatively large median Dst_{min} values with a median value of -157 nT for group (a) (all multiple CME cases) and -181 nT for group (d) (multiple CME with > 3 CMEs). Group (c) (CIR cases) and group (e) (cases with HSS involved) exhibited modest median intensity with a median Dst_{min} of -115 nT and -133 nT, respectively. In the multiple CME group (d), the CME interaction may play an important role in enhancing the intensity of the LLGMS events. Figure 9b shows the relationship between the LLGMS intensity and the degree of interaction (ni) (see definition in Section 3). It is found that the correlation coefficient (r) between the intensity and ni is 0.67.

4.3 Preconditioning in LLGMS Events

The relationship of the intensity of magnetic storms to solar wind parameters can be examined using the Burton's equation [Burton *et al.*, 1975]. Burton's equation has been tested and improved by numerous authors [e.g., Clua de Gonzalez & Gonzalez, 1998; Fenrich and Luhman, 1998; O'Brien and McPherron, 2000; Wang *et al.*, 2003]. It is given by O'Brien and McPherron in a slightly different form:

$$\frac{dDst^*}{dt} = Q(t) - \frac{Dst^*(t)}{\tau}, \quad (6)$$

where the energy injection term $Q = \begin{cases} a(VB_s - E_c) & VB_s > E_c \\ 0 & VB_s < E_c \end{cases}$, V is the solar wind flow speed,

VB_s is the solar wind dawn-dusk electric field, the proportional constant a is $-4.4 \text{ nT/h(mV/m)}^{-1}$ and the electric field threshold E_c is 0.49 mV/m . The pressure-corrected index

$Dst^* = Dst - b\sqrt{p} + c$, from which the contribution of the magnetopause current to Dst has been removed, p is the solar wind dynamic pressure, b is a constant of proportionality, and c is a constant representing the changes of both the quiet time magnetopause and the ring currents, and τ is the decay time of the ring current, associated with loss processes in the inner magnetosphere. O'Brien and McPherron's improved model has also considered the influence of VB_s on τ as follows: $\tau = 2.40 \exp [(9.74/4.69 + VB_s)]$ with VB_s in mV/m . More recently, Wang et al. [2003] suggested that the O'Brien and McPherron's model can be further improved by $Q = a(VB_s - E_c)(p/p_0)^\gamma$, where the index γ and the constant p_0 are optimized by minimizing the root-mean-square (RMS) errors.

The empirical Dst model combined with the statistically derived decay time have had remarkable success in predicting the strength of geomagnetic storms [see review by *Gonzalez et al.* 1994]. However, Burton's formula and its variations [e.g., *O'Brien & Mcpherron*, 2000; *Wang et al.*, 2003] depend only on the solar wind coupling value VB_s and does not take into account any preexisting condition in the magnetosphere, so they might not be applicable for the multi-step Dst development of LLGMS events when preconditioning occurs due to the presence of successive storms. In order to investigate whether Burton's formula and its variations are applicable for the Dst development of LLGMS, we studied the relationship between B_s , VB_s , and Dst_{min} . We divided the LLGMS events as individual ring current intensifications, i.e., individual Dst dips in the main and recovery phases. We identify the Dst

dips according to the following conditions: 1) Dst_{min} must be less than -50 nT; 2) two consecutive dips must be separated by more than 3 hours; 3) the magnitude of the decrease of Dst_{min} in a dip must be less than -30 nT or Dst_{min} remains the same level (see Figure 3 as an example) for more than 6 hours. We use the first criterion to exclude weak storms, which are mostly caused by HSS events. The second criterion excludes cases in which apparent decreases in Dst were caused by substorm effects such as the so-called current wedge, not a true increase in the storm time ring current [Kamide *et al.*, 1998]. The third criterion is employed to help distinguish a well-defined dip.

Figure 10 shows the relationship between Dst_{min} , B_s , and VB_s . From top to bottom, this figure shows the results for: all Dst dips, Dst dips in the main phase, and Dst dips in the recovery phase, respectively. As expected, in general, Dst_{min} is well correlated with B_s ($r=0.79$) and VB_s ($r = 0.80$). In the main phase, Dst_{min} has a better correlation with both B_s ($r = 0.79$) and VB_s ($r = 0.84$). In the recovery phase, however, the correlation relation between Dst_{min} , B_s , and VB_s is relatively poor, with coefficients of 0.59 and 0.60, respectively. The results imply that in the main phase the preconditioning of previous storms may not play a significant role in the multiple development of Dst since each Dst dip acts as a separately existing storm in this stage. However, in the recovery phase the effect of preconditioning on the Dst development cannot be ignored. This is due to the fact that in the recovery phase the Dst recovery and Dst decay (of later consecutive storms after Dst negative peak) occurs at the same time in the LLGMS events. After the maximum intensification of the ring current, the cumulative effects of prior storms on plasma sheet characteristics will change the response of the magnetosphere to solar wind drivers, as proposed by Kozyra *et al.* [1998, 2002].

5. Summary and Discussion

We investigated 37 LLGMS events from 1998 to 2002. We find three causes of LLGMS events: 1) Multiple CMEs (64.9%, 24 of 37); 2) Single CME (21.6%, 7 of 37); 3) HSS in CIRs (13.5%, 5 of 37). The first two causes of LLGMS events involved possible HSS events, causing complex interaction regions in the interplanetary medium. In the multiple CME cases, the associated IP driver is a merged interaction region involving IP shock, complex ejecta, and HSS. The LLGMS events involving multiple CME have medium long duration and high intensity due to successive CMEs and various interactions. The single CME cases generally involve a fast halo CME associated with a very strong interplanetary shock, which produces super intensity (> -280 nT) storm. In the CIR cases, the LLGMS events have modest intensity (~ 100 nT) but the longest duration due to extended periods of the highly fluctuating B_s within HSS.

If an LLGMS is associated with interacting CMEs, there is a good correlation between the number of CMEs involved in an LLGMS and the LLGMS duration with correlation coefficient $r = 0.78$. Interaction between successive CMEs plays an important role in enhancing the intensity of the LLGMS events. The intensity of LLGMS is well correlated with the degree of interaction (i.e., the number of CMEs interacting with HSS or with themselves in the associated interaction region) with $r = 0.67$. Of the 37 LLGMS events we studied, there were 20 (54.1%) events involving possible CME interaction. The largest LLGMS during 1998-2002 is the 2001 March 31 event with $Dst_{min} \sim -387$ nT, which was involved four successive CMEs interacting with one another. Note that there are cases of interacting CMEs which do not trigger LLGMS due to unfavorable northward IMF conditions. Our analysis does not include these cases because we are interested in the solar origin of the existing LLGMS.

As we expected, there is a good correlation between Dst_{min} , B_s , and VB_s . The correlation of Dst_{min} with B_s for all the dips in LLGMS events is 0.77 and for the dips in the main phases it is 0.79. The correlation of Dst_{min} with VB_s is slightly better than with B_s with $r = 0.80$ and 0.84, respectively, for all dips and main phase dips. However, in the recovery phases, the correlation relation is relatively poor, with coefficients of 0.59 and 0.60 between Dst_{min} and B_s , VB_s , respectively.

Our results suggest that the preconditioning may have little effect on multiple Dst development in the main phase of LLGMS, while it does affect the recovery phase. The reason is that the recovery phase involves both the ring current decay of prior storms and intensification of later storms in an LLGMS event. After the Dst negative peak, the cumulative effects of prior storms on plasma sheet characteristics will alter the response of the magnetosphere to subsequent solar wind drivers, as suggested by *Kozyra et al.* [1998, 2002]. However, how the plasma sheet responds to the solar wind driver and how it is affected by the preexisting storms are still not well understood. Further detailed investigation on the preconditioning is needed.

Acknowledgments: The authors would like to thank the support of ACE/SWICS, ACE/SWEPAM, WIND/MFI teams and NSSDC center for processing data. This work was supported by NASA LWS and NSF SHINE (ATM 0204558) program. AL thanks UNAM grant PAPIIT IN119402 for partial support.

References

Brueckner, G. E., J. P. Delaboudiniere, R. A. Howard, S. E. Paswaters, O. C. St. Cyr, R. Schwenn, P. L. Lamy, G. M. Simnett, B. Thompson, D. Wang, Geomagnetic storms caused

- by coronal mass ejections (CMEs): March 1996 through June 1997, *Geophys. Res. Lett.*, 25, 3019, 1998.
- Burlaga, L. F., Interplanetary stream interfaces, *J. Geophys. Res.*, 79, 3717 – 3725, 1974.
- Burlaga, L. F., K. W. Behannon and L. W. Klein, Compound streams, magnetic clouds, and major geomagnetic storms, *J. Geophys. Res.*, 92, 5725-5734, 1987.
- Burlaga, L. F., Interplanetary magnetohydrodynamics, New York: Oxford University Press, 1995.
- Burlaga, L. F., S. P. Plunkett and O. C. St. Cyr, Compound streams, successive CMEs and complex ejecta, *J. Geophys. Res.*, 107, SHH 1-1, 2002.
- Burlaga, L., D. Berdichevsky, N. Gopalswamy, R. Lepping and T. Zurbuchen, Merged interaction regions at 1 AU, *J. Geophys. Res.*, 108, SHH 2-1, 2003.
- Cane, H. V. and I. G. Richardson, What caused the large geomagnetic storm of November 1978? *J. Geophys. Res.*, 120, 17445 – 17450, 1997.
- Cane, H. V., I. G. Richardson, O. C. St. Cyr, O. C., Coronal mass ejections, interplanetary ejecta and geomagnetic storms, *Geophys. Res. Lett.*, 27, 3591, 2000.
- Chen, M. W., L. R. Lyons, and M. Schulz, Stormtime ring-current formation: A comparison between single-and double-dip model storms with similar transport characteristics, *J. Geophys. Res.*, 106, 27755, 2000.
- Clua de Gonzalez, A. L. and W. D. Gonzalez, Analytical study of the energy rate balance equation for the magnetospheric storm-ring current, *Ann. Geophysicae*, 16, 1445, 1998.
- Crooker, N. U., J. T. Gosling and S. W. Kahler, Magnetic clouds at sector boundaries, *J. Geophys. Res.*, 103, 301 - 306, 1998.
- Daglis, I. A., The role of magnetosphere-ionosphere coupling in magnetic storm dynamics, in Magnetic Storms, *Geophys. Monogr.* 98, edited by. B. T. Tsurutani, W. D. Gonzalez, Y. Kamide, and J. K. Arballo, pp.107, American Geophysical Union, Washington, DC, 1997.
- Dasso, S., D. Gomez, and C. H. Mandrini, Ring current decay rates of magnetic storms: a statistical study for 1957 to 1998, *J. Geophys. Res.*, 107, SMP5, 2002.

- Fenimore, E. E., Solar wind flows associated with hot heavy ions, *Astrophys. J.*, 235, 245, 1980.
- Fenrich, F. R., and J. G. Luhmann, Geomagnetic response to magnetic clouds of different polarity, *Geophys. Res. Lett.*, 25, 2999-3002, 1998.
- Gloeckler, G., et al., Unusual composition of the solar wind in the 2-3 May 1998 CME observed with SWICS on ACE, *Geophys. Res. Lett.*, 26, 157, 1999.
- Gonzalez, W. D., J. A. Joselyn, Y. Kamide, H. W. Kroehl, G. Rostoker, B. T. Tsurutani, and V. M. Vasylunas, What is a geomagnetic storm?, *J. Geophys. Res.*, 99, 5771 - 5792, 1994.
- Gonzalez, W. D., A.L., Clua de Gonzalez, J. H. A., Sobral, A. Dal Lago, L. E., Vieira, Solar and interplanetary causes of very intense geomagnetic storms, *J. Atmospheric Terrest. Phys.*, 63, 403 – 412, 2001.
- Gopalswamy, N., A. Lara, R. P. Lepping, M. L. Kaiser, D. Berdichevsky, O. C. St. Cyr, Interplanetary acceleration of coronal mass ejections, *Geophys. Res. Lett.*, 27, 145, 2000.
- Gopalswamy, N., A. Lara, S. Yashiro, M. L. Kaiser and R. A. Howard, Predicting the 1-AU arrival times of coronal mass ejections, *J. Geophys. Res.*, 106, 29207- 29217, 2001.
- Gopalswamy, N., Relation Between Coronal Mass Ejections and their Interplanetary Counterparts, Solar-Terrestrial Magnetic Activity and Space Environment, Proceedings of the COSPAR Colloquium held in the NAOC in Beijing, China, September 10-12, 2001. Edited by Huaning Wang and Ronglan Xu. 1st ed. Boston: Pergamon, 2002. COSPAR colloquia series; v. 14, p.157, 2002.
- Gopalswamy, N., S. Yashiro, G. Michalek, H. Xie, R. P. Lepping, and R. A. Howard, Solar source of the largest geomagnetic storm of cycle 23, *Geophys. Res. Lett.*, in press.
- Grande, M., C. H. Perry, J. B. Blake, M. W., Chen, J. F. Fennell and B. Wilken, Observations of iron, silicon, and other heavy ions in the geostationary altitude region during late March 1991, *J. Geophys. Res.*, 101, 24707- 24718, 1996.

- Hamilton, D. C., G. Gloeckler, F. M. Ipavich, B. Wilken, and W. Stuedemann, Ring current development during the great geomagnetic storm of February 1986, *J. Geophys. Res.*, **93**, 14343, 1988.
- Henke, T., et al., Differences in the O^7/O^6 ratio in magnetic cloud and non-cloud coronal mass ejections, *Geophys. Res. Lett.*, **25**, 3465, 1998.
- Kamide, Y., N. Yokoyama, W. Gonzalez, B. T. Tsurutani, I. A. Daglis, A. Brekke, S. Masuda, Two-step development of geomagnetic storms, *J. Geophys. Res.*, **103**, 6917-6922, 1998.
- Kozyra, J. U., J. E. Borovsky, M. W. Chen, M.-C. Fok, and V. K. Jordanova, Plasma sheet preconditioning, enhanced convection and ring current development, in *Substorms-4*, edited by S. Kokubun and Y. Kamide, 755-760, *Terra Sci.*, Tokyo, 1998.
- Kozyra, J. U., M. W. Liemohn, C. R. Clauer, A. J. Ridley, M. F. Thomsen, J. E. Borovsky, J. L. Roeder, V. K. Jordanova, and W. D. Gonzalez, Multistep Dst development and ring current composition changes during the 4-6 June 1991 magnetic storm, *J. Geophys. Res.*, **107**, 1224, 2002.
- Lepping, R. P., D. B. Berdichevsky, C.-C. Wu, A. Szabo, T. Narock, F. Mariani, A. J. Lazarus, and A. J. Quivers, A summary of WIND magnetic clouds for year 1995 – 2003: Model-fitted parameters, associated errors, and classifications, *Ann. Geophys.*, submitted, 2005.
- Lepri, S. T., T. H. Zurbuchen, L. A. Fisk, I. G. Richardson, H. V. Cane, and G. Gloeckler, Fe charge distributions as an identifier of interplanetary coronal mass ejections, *J. Geophys. Res.*, **106**, 29,231, 2001.
- Manoharan, P.K., N. Gopalswamy, S. Yashiro, A. Lara, G. Michalek, R. A. Howard, Influence of coronal mass ejection interaction on propagation of interplanetary shocks, *J. Geophys. Res.*, **109**, A06109, 2004.
- O'Brien, T. P., and R. L. McPherron, An empirical phase space analysis of ring current dynamics: Solar wind control of injection and decay, *J. Geophys. Res.*, **105**, 7707, 2000.

- Tsurutani, B. T. and W. D. Gonzalez, The interplanetary causes of magnetic storms, in Magnetic Storms, *Geophys. Monogr.*, 98, edited by B. T. Tsurutani, W. D. Gonzalez, Y. Kamide, and J. K. Arballo, pp.77, American Geophysical Union, Washington, DC, 1997.
- Wang, C. B., J. K. Chao, and C.-H. Lin, Influence of the solar wind dynamic pressure on the decay and injection of the ring current, *J. Geophys. Res.*, 108, 1341, 2003.
- Wang, Y. M., P. Z. Ye, S. Wang, G. P. Zhou, J. X. Wang, Statistical study on the geoeffectiveness of Earth-directed coronal mass ejections from March 1997 to December 2000, *J. Geophys. Res.*, 107, pp. SSH 2-1, 2002.
- Webb, D. F., E. W. Cliver, N. U. Crooker, O. C. St. Cyr, B. J. Thompson, Relationship of halo coronal mass ejections, magnetic clouds, and magnetic storms, *J. Geophys. Res.*, 105, 7491-7508, 2000.
- Xie, H., L. Ofman, and G. Lawrence, Cone Model for Halo CMEs: Application to Space Weather Forecasting, *J. Geophys. Res.*, Volume 109, Issue A3, 2004.
- Yashiro, S., N. Gopalswamy, G. Michalek, O. C. St. Cyr, S. P. Plunkett, N. B. Rich, and R. A. Howard, A Catalog of White Light Coronal Mass Ejections Observed by the SOHO Spacecraft, *J. Geophys. Res.*, 109, A07105, 2004.
- Zhang et al., Identification of solar sources of major geomagnetic storms between 1996 and 2000, *Astrophys. J.*, 582, 520-533, 2003.

H. Xie, N. Gopalswamy, P.K. Manoharan, A. Lara, S. Yashiro, and S. Lepri, The Catholic University of America/NASA Goddard Space Flight Center, Code 682, Greenbelt, MD 20771, USA.

(hong@lepvax.gsfc.nasa.gov, gopals@fugee.gsfc.nasa.gov, mano@ncra.tifr.res.in,
alara@kin.igeofcu.unam.mx, yashiro@cdaw.gsfc.nasa.gov, slepri@umich.edu)

Figure 1. Topology of the cone model. The coordinate (x_h, y_h, z_h) is the heliocentric coordinate system, where z_h points to Earth, y_h points north, and the $x_h - y_h$ plane defines the plane of the sky (POS). The coordinate (x_c, y_c, z_c) is the cone coordinate system, where x_c is the cone axis, and the $y_c - z_c$ plane is parallel to the base of the right cone. The angles (ϕ, λ) are the longitude and latitude relative to the ecliptic plane. λ is the angle between the cone axis x_c and the $x_h - y_h$ plane and ϕ is the angle between projection of x_c on the $x_h - y_h$ plane x_c' and the $z_h -$ axis. The angles (α, θ) are defined as the longitude and latitude relative to POS for conveniently determining the cone model parameters, where θ is the angle between x_c and POS and α is the angle between the cone axis projection on POS and $x_h -$ axis.

Figure 2. Illustration of the constraint $\omega \geq \beta + \Delta$ between the angular width 2ω and orientation (β, Δ) for a front-side halo ($\Delta = 0$) or partial halo CME to encounter Earth. O is the solar disk center. O' is any arbitrary point on the solar surface near the disk center. β is the angle between the cone central axis and the line-of-sight (LOS). θ is the angle between the cone central axis and the plane of the sky. L is the distance of O' to the LOS, and Δ is the angle between the LOS and one (Earth-directed) of the cone lateral projections.

Figure 3. (a) A LLGMS associated with successive CMEs. From top to bottom: the panels are D_{st} Index, Fe charge state, $|B|$, B_z , N , T , V and CME height-time profile,

respectively. The vertical solid lines indicate the ICME shock front ($F_1, 2, 3, 4, F$ denotes forward fast shock). The number on the bottom panel indicates the associated CMEs. The arrows show the dips in complex structures of D_{st} and B_z . Note that the drop in $\langle Q_{Fe} \rangle$ near F_2 is due to the instrumental noise produced by the impact of the shock.

Figure 3. (b) LASCO C2 images of CMEs associated with the event. From top left to bottom right: CME 1, CME2, CME3, and CME 4.

Figure 4. (a) A LLGMS associated with two IMCs. From top to bottom: the panels are D_{st} Index, Fe charge state, $|B|$, B_z , N , T , V and CME height-time profile, respectively. The vertical solid lines indicate the ICME shock front (F_1, F_2, R_2 , F denotes forward fast shock and R denotes reverse shock). The number on the bottom panel indicates the associated CMEs. The arrows show the dips in complex structures of D_{st} and B_z .

Note that the drop in $\langle Q_{Fe} \rangle$ near F_1 due to the instrumental noise produced by the impact of the shocks.

Figure 4. (b) LASCO C2 images of CME 1 and CME 2 associated with the event.

Figure 5. A LLGMS associated with a single CME event: corresponding solar wind data, IMF, and the D_{st} index from Apr-02-2000 ~ Apr-11-2000. The associated CME is a fast Halo with an actual speed of 1139 km/s.

Figure 6. A LLGMS associated with a HSS event: corresponding solar wind data, IMF, and the D_{st} index from Oct-04-2002 ~ Oct-13-2002. There was a coronal hole a few days earlier near the disk center at 22:00 UT in the Oct-05-2002 EIT image (not shown).

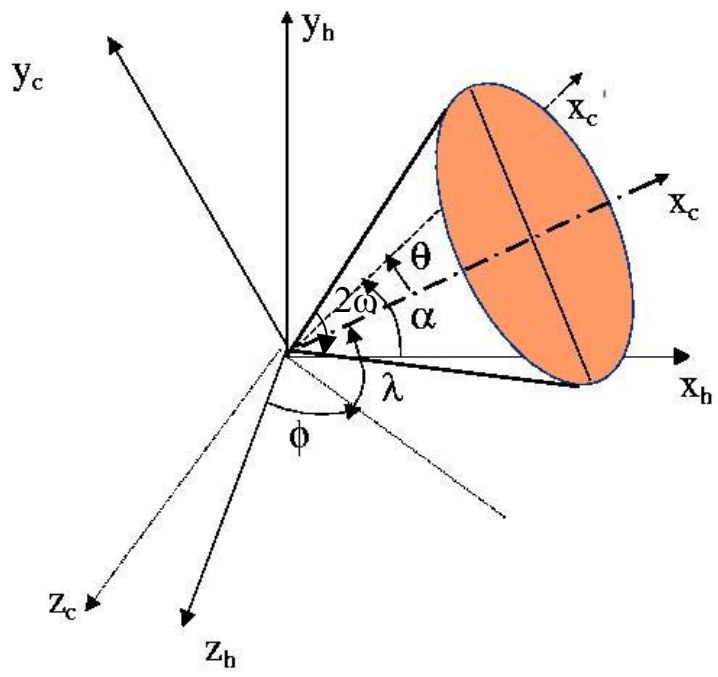
Figure 7. Histograms of durations for the six groups of LLGMS events. These six groups are: (a) all multiple CME cases; (b) all single CME cases; (c) all CIR cases with no related CME;

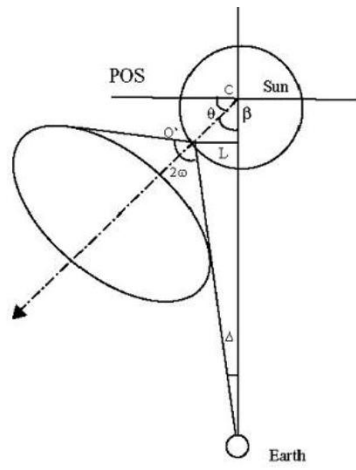
(d) Multiple CME cases with > 3 CMEs; (e) all cases with HSS involved; (f) cases with no HSS and ≤ 2 CMEs.

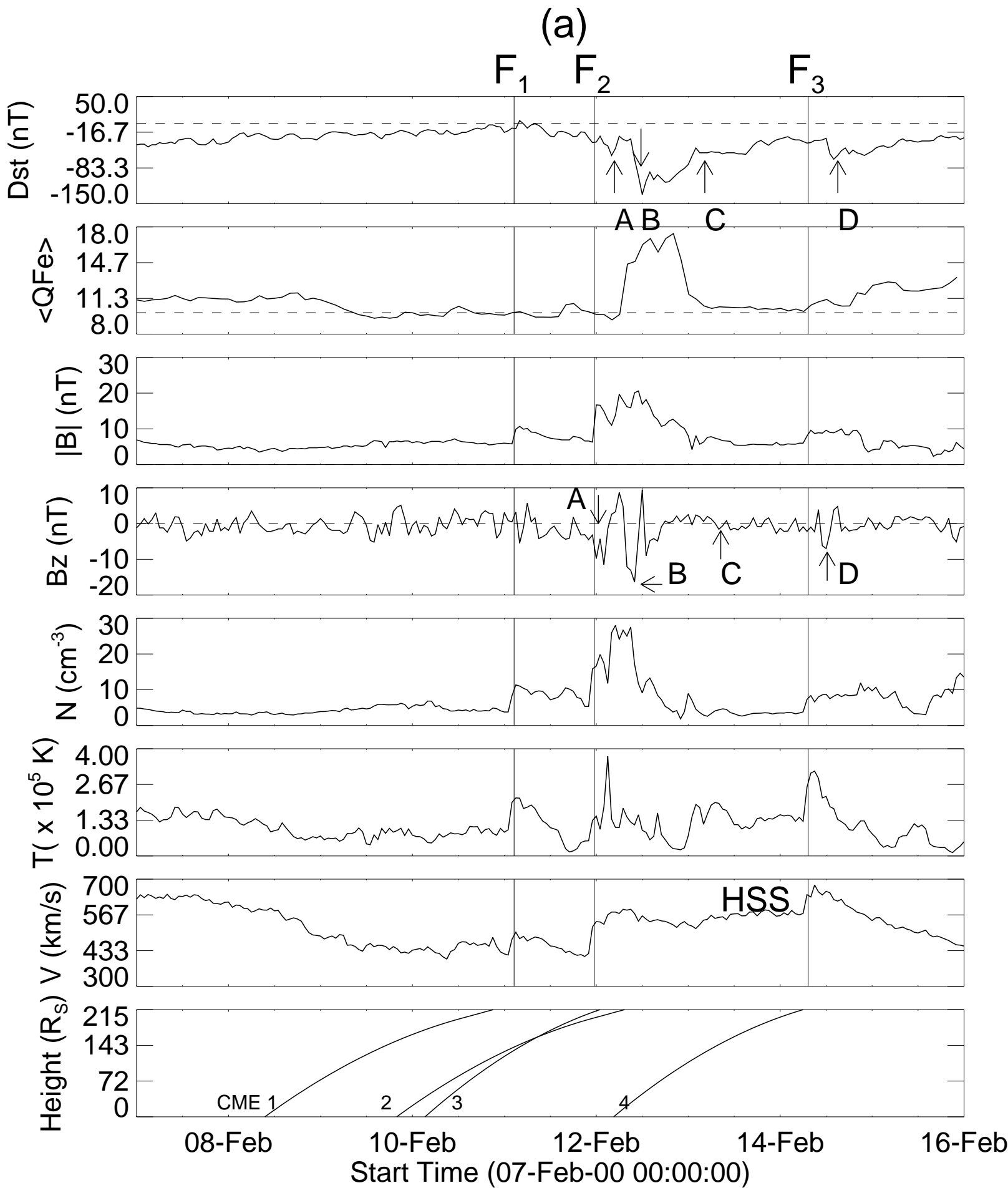
Figure 8. Histograms of Dst minimums (absolute value) for the six groups of LLGMS events. These six groups are: (a) all multiple CME cases; (b) all single CME cases; (c) all CIR cases with no related CME; (d) Multiple CME cases with > 3 CMEs; (e) all cases with HSS involved; (f) cases with no CME interaction.

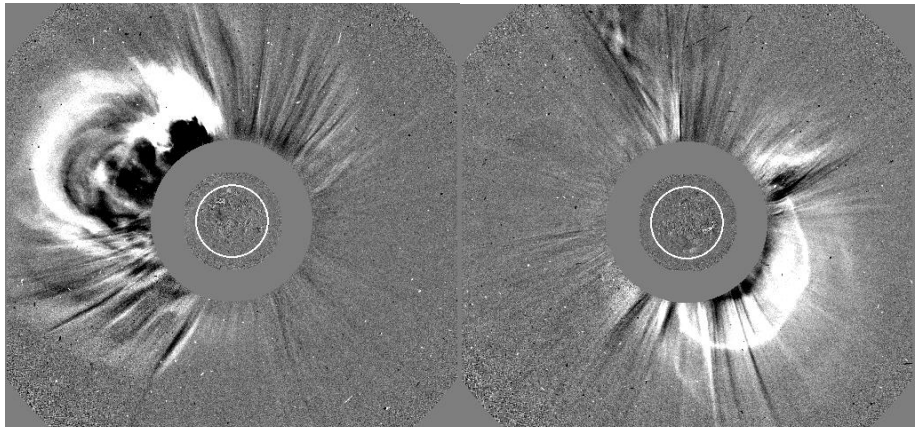
Figure 9. Relationships and correlation coefficients for (a) LLGMS duration and the number of associated CMEs (nc); b) LLGMS intensity and the degree of interaction (ni).

Figure 10. Relationships of Dst_{min} with B_s and VB_s . From top to bottom, panels are the results for all dips in LLGME events, dips in main phases, and dips in recovery phases, respectively.

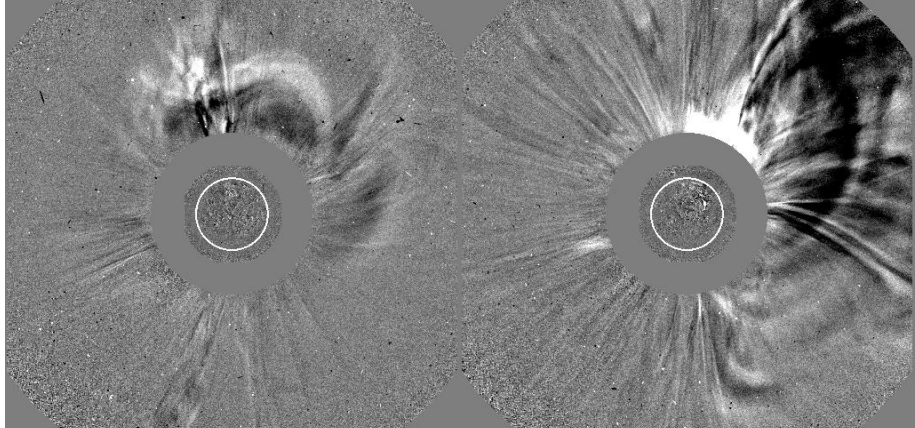






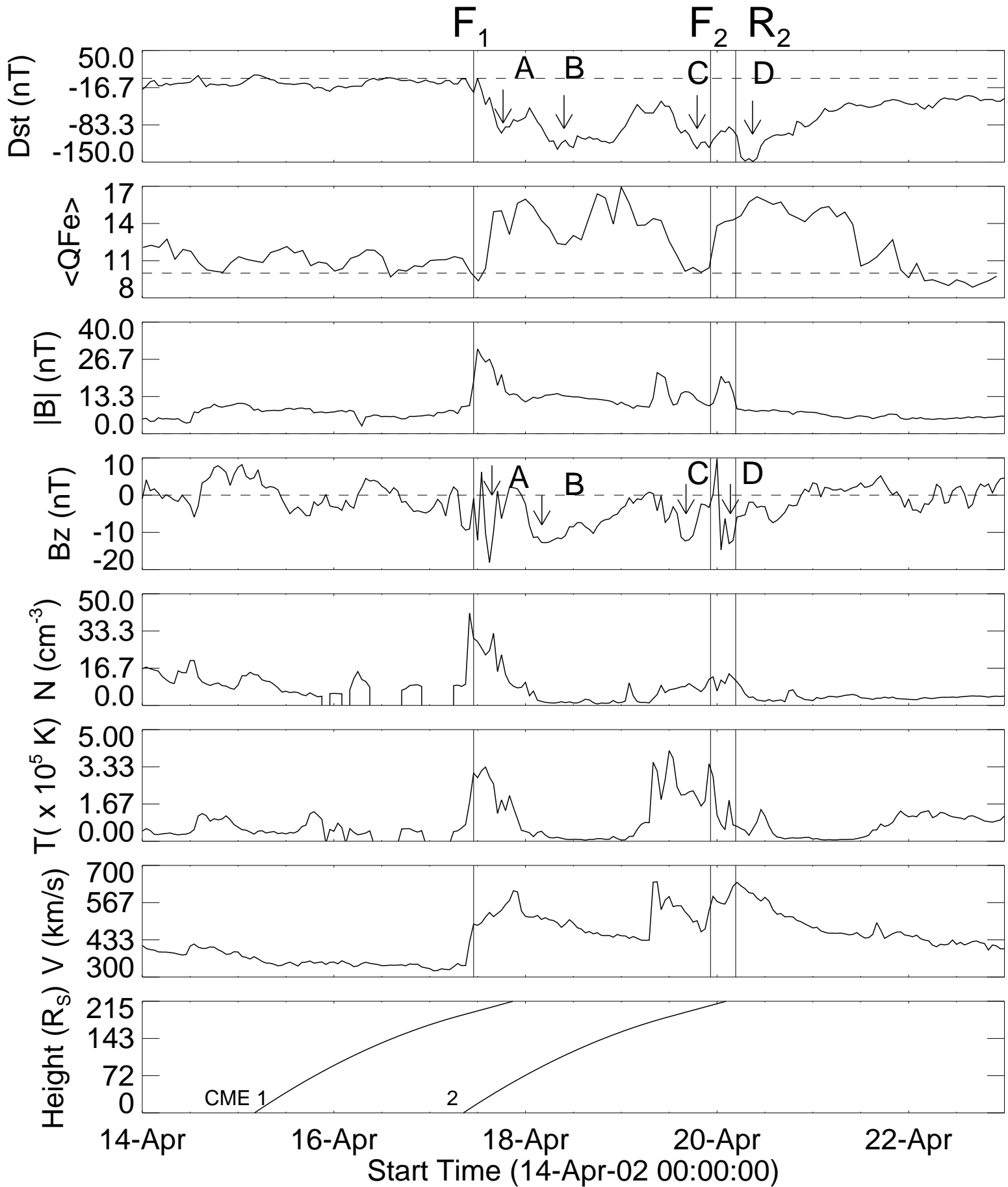


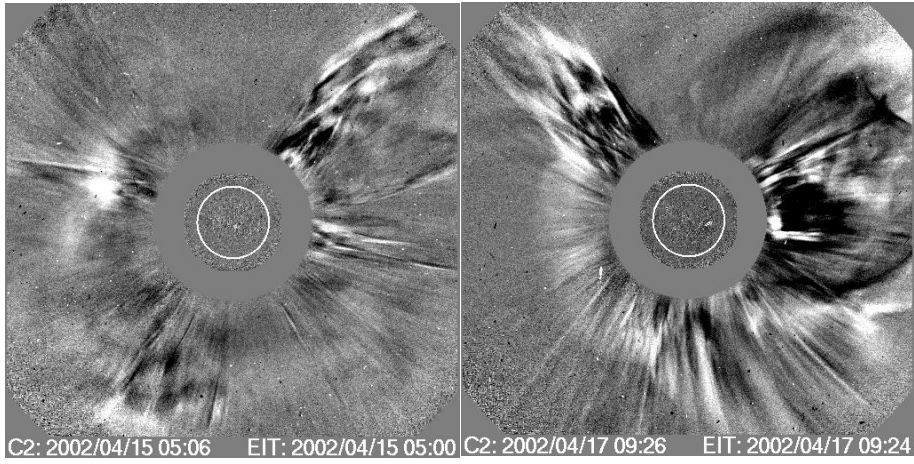
C2: 2000/02/08 10:06 EIT: 2000/02/08 10:00 C2: 2000/02/09 20:30 EIT: 2000/02/09 20:24

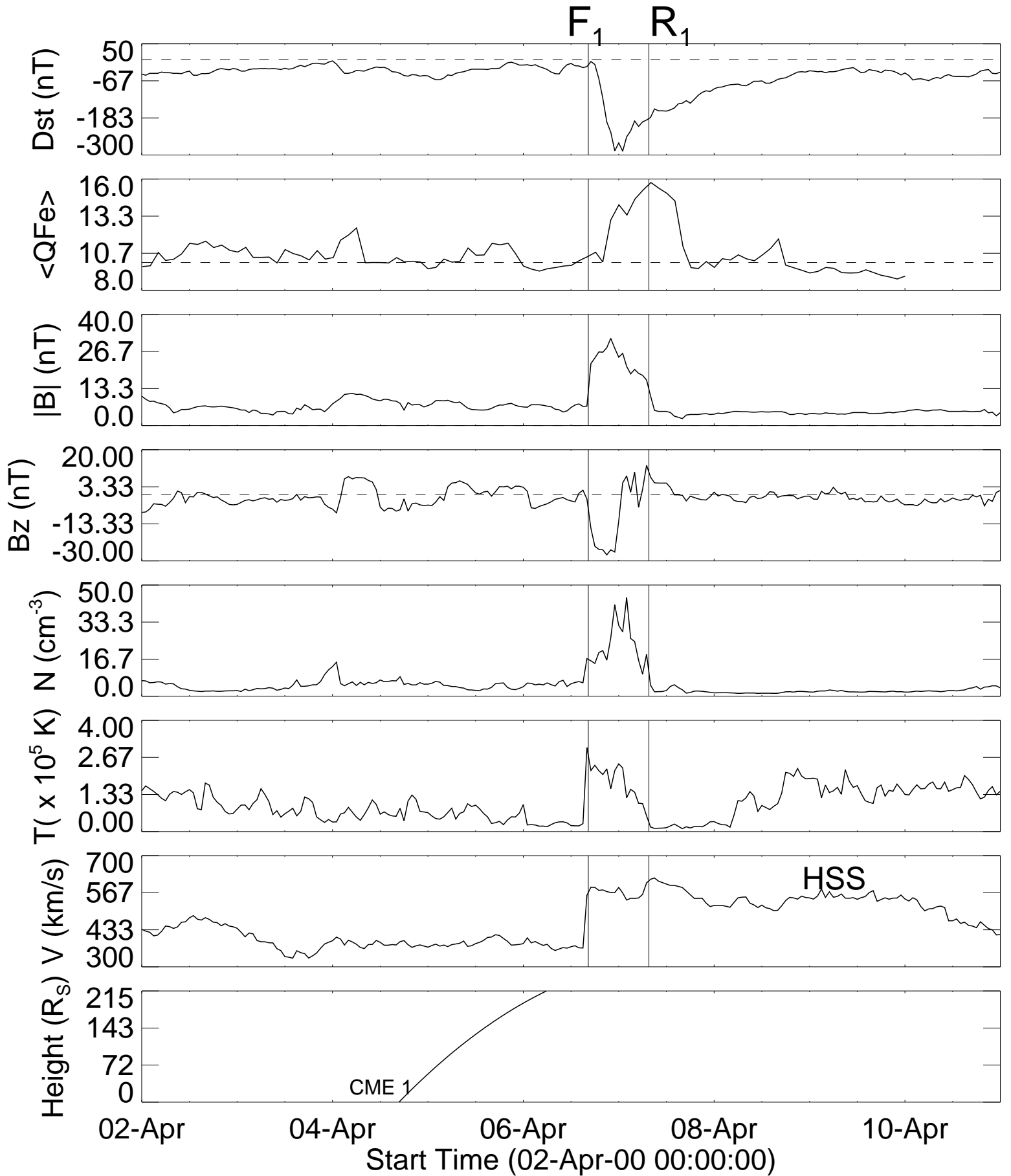


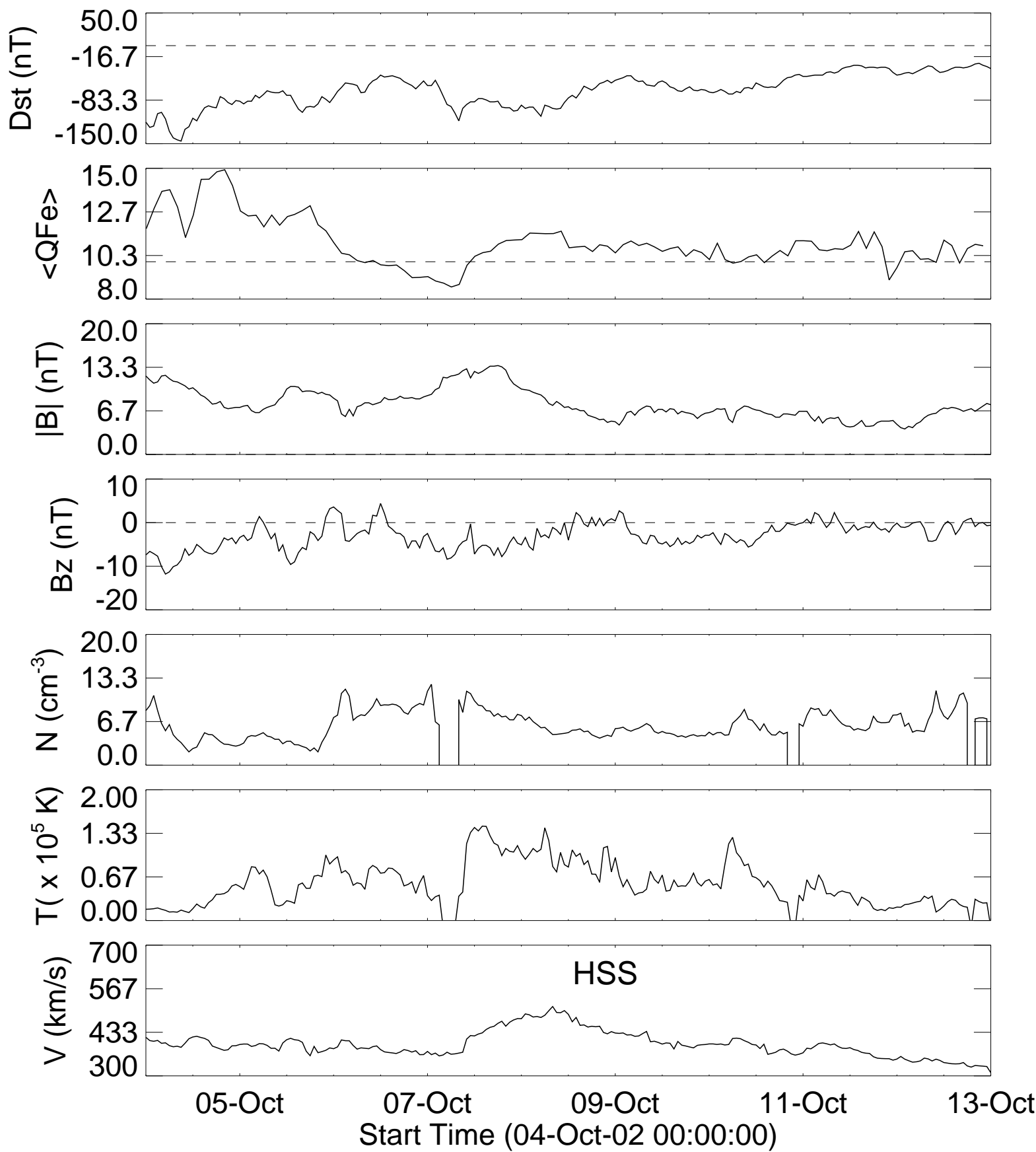
C2: 2000/02/10 03:06 EIT: 2000/02/10 03:00 C2: 2000/02/12 04:31 EIT: 2000/02/12 04:25

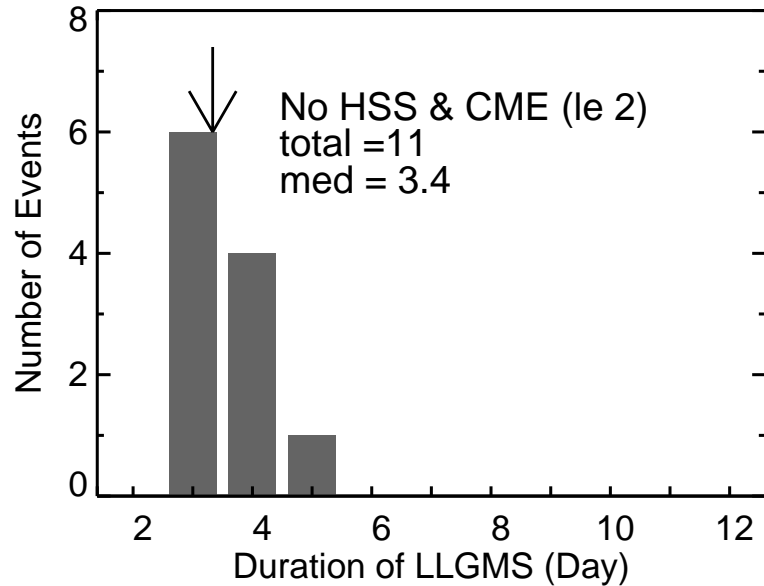
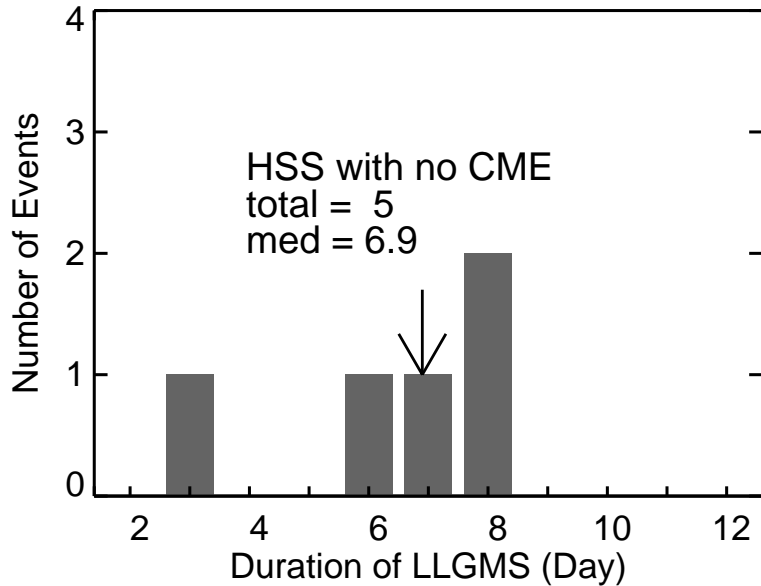
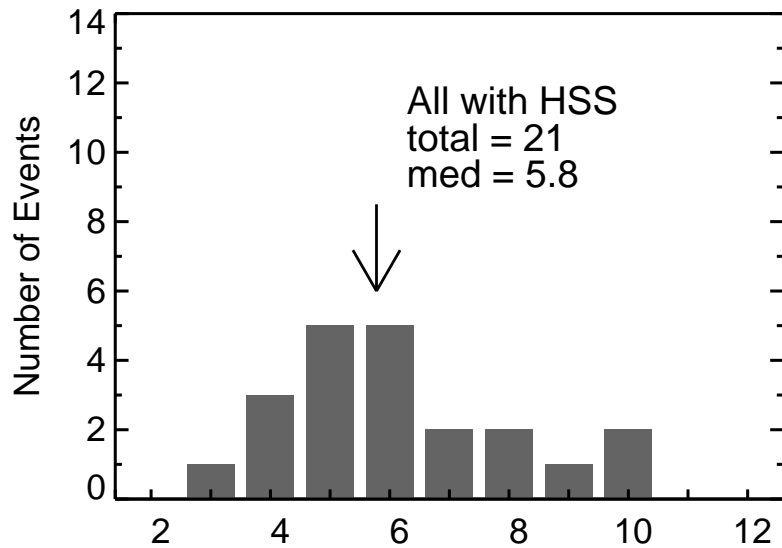
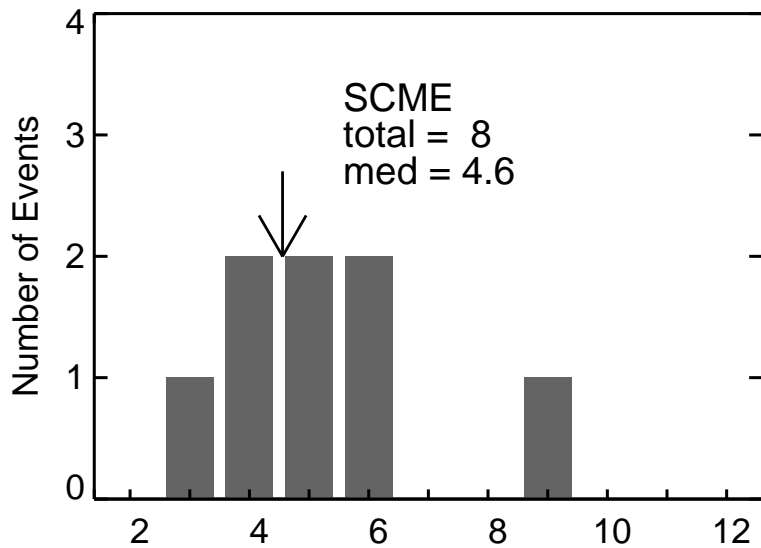
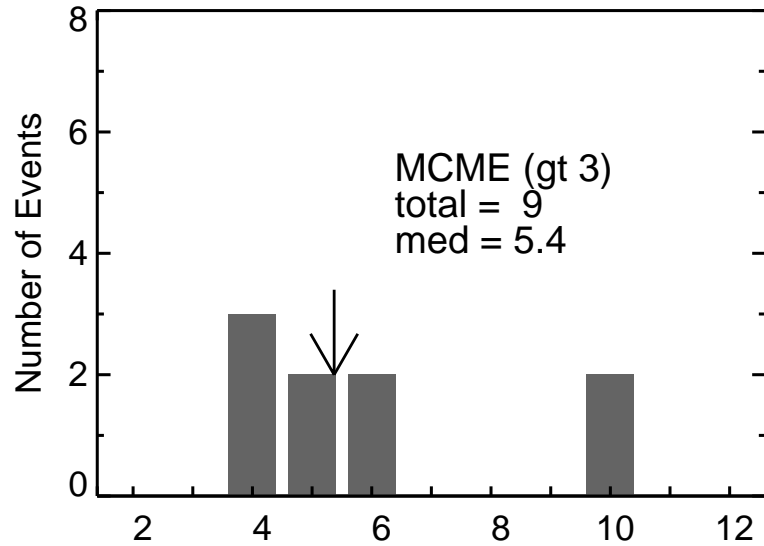
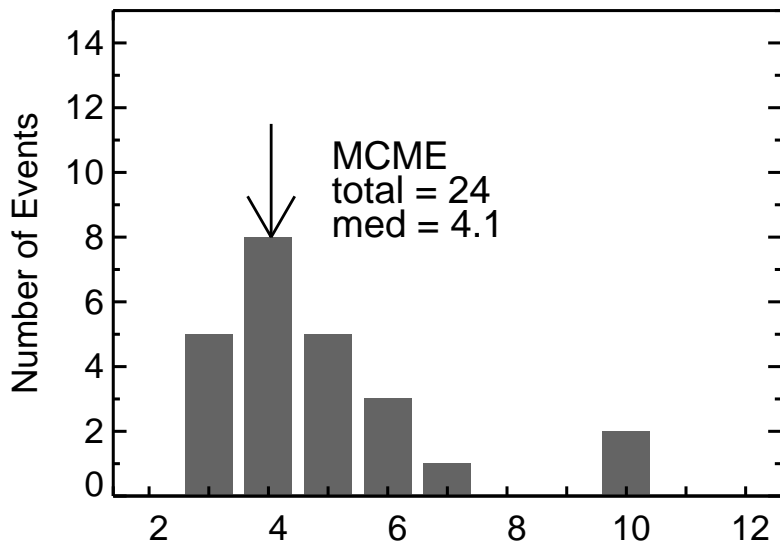
(a)

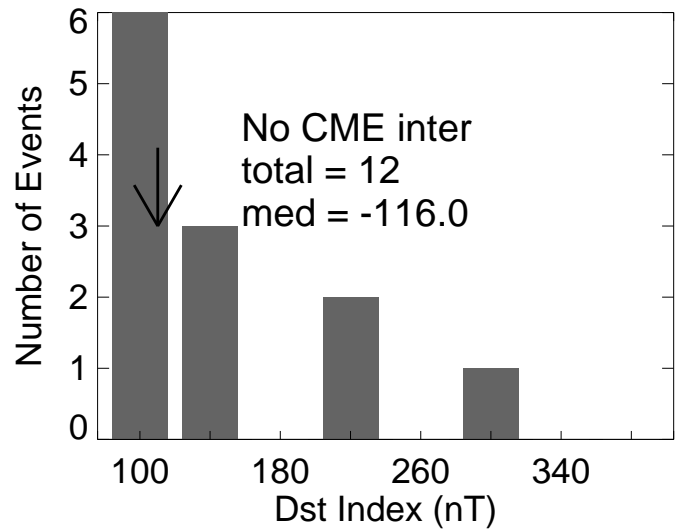
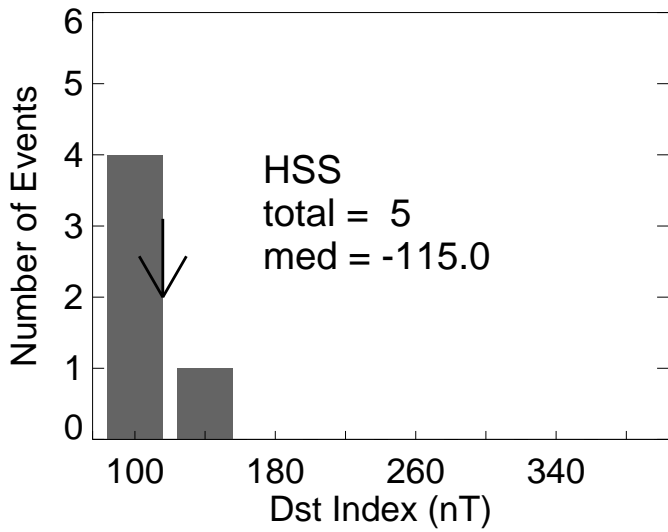
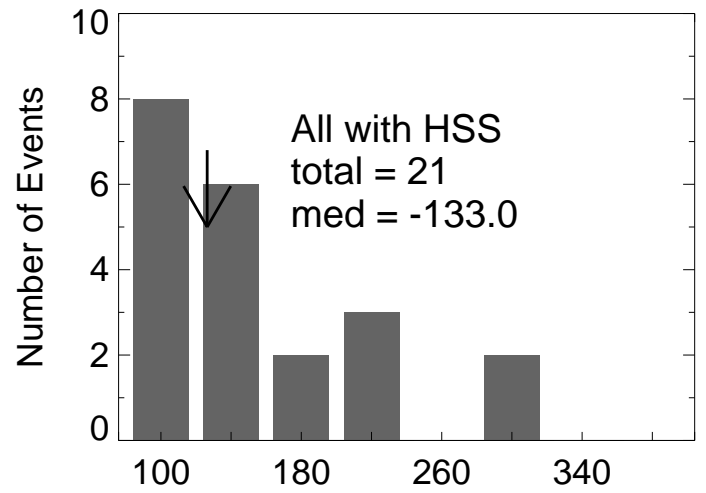
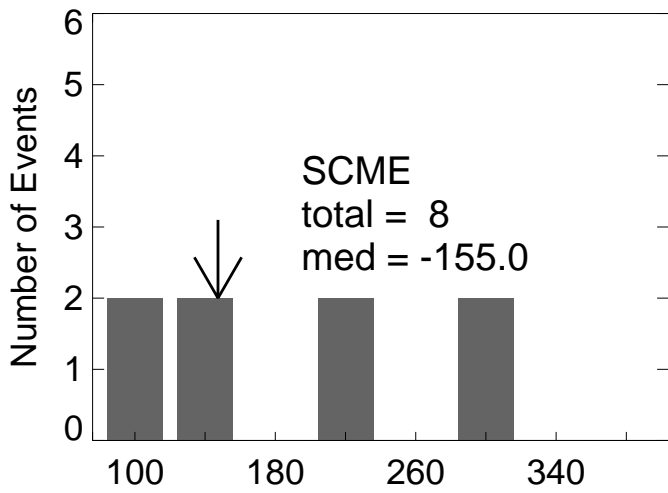
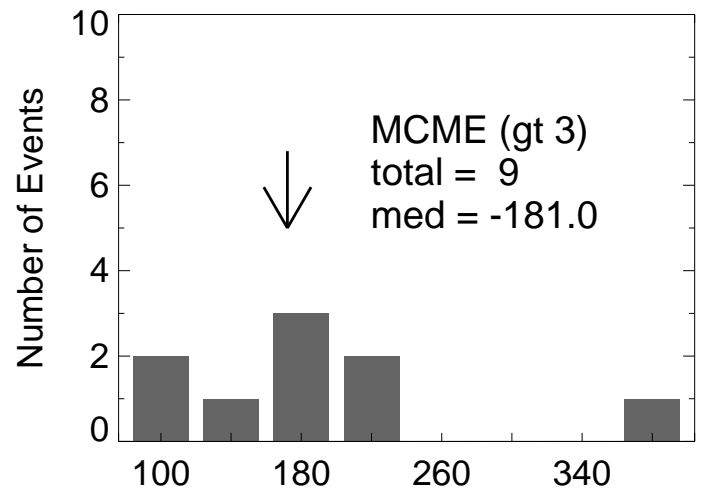
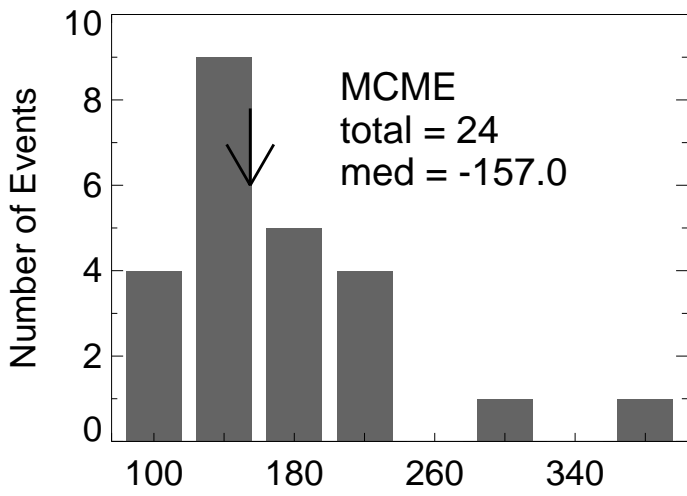




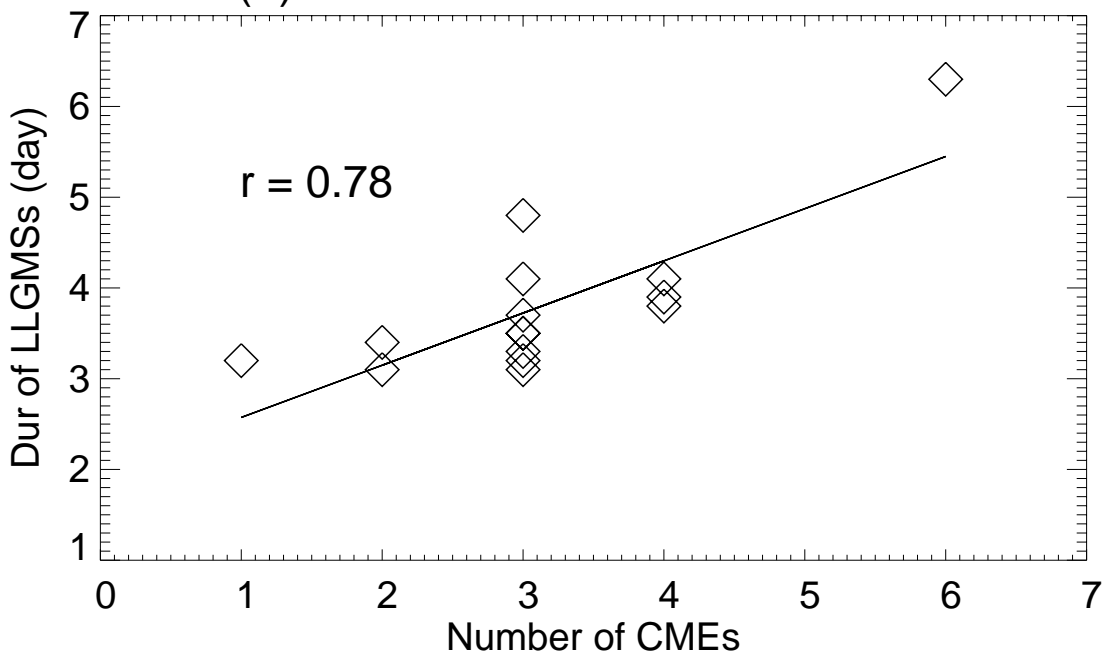




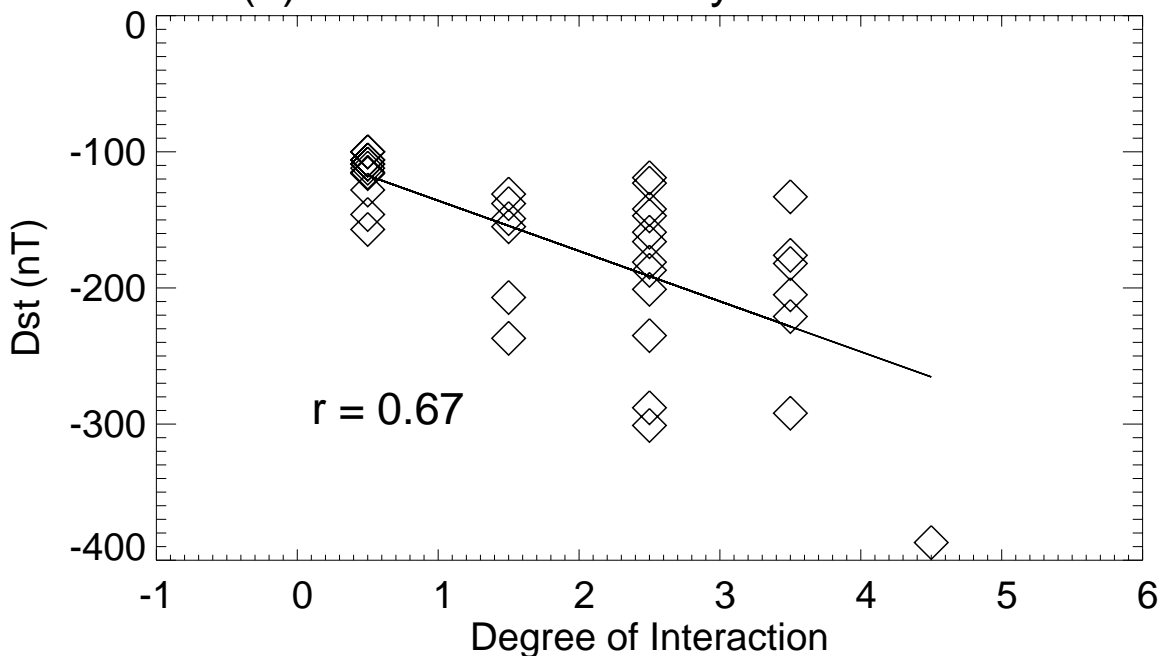




(a) Relation of Duration vs. CMEs



(b) Relation of Intensity vs. Interaction



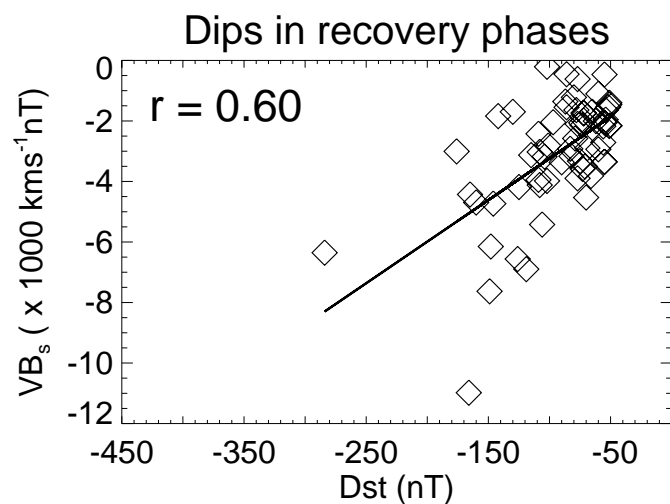
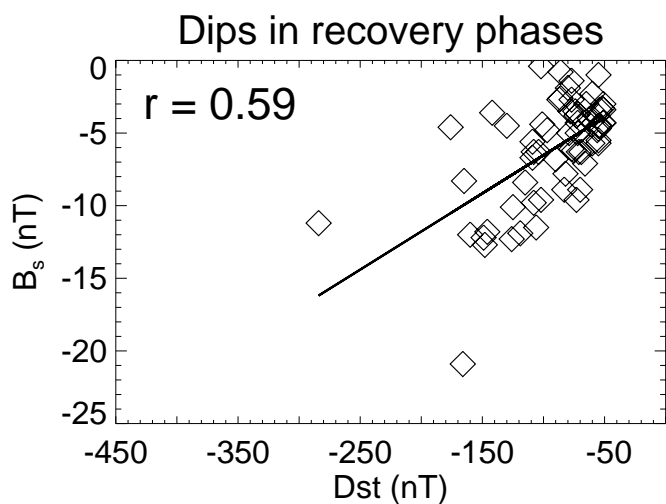
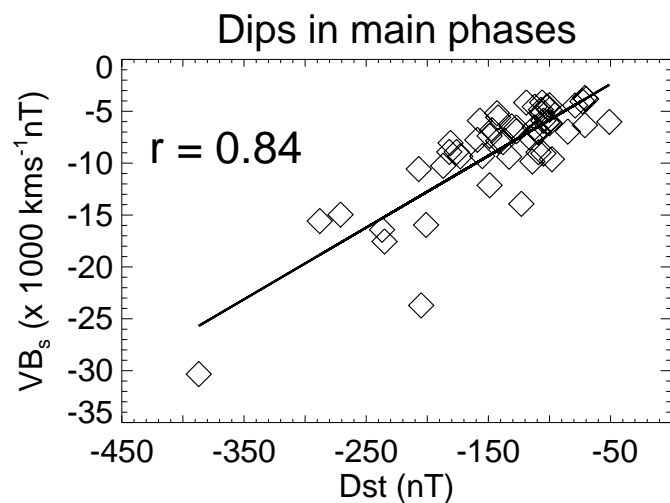
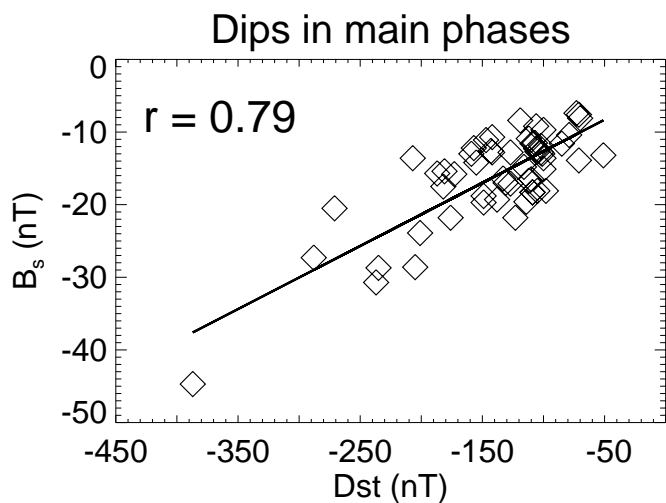
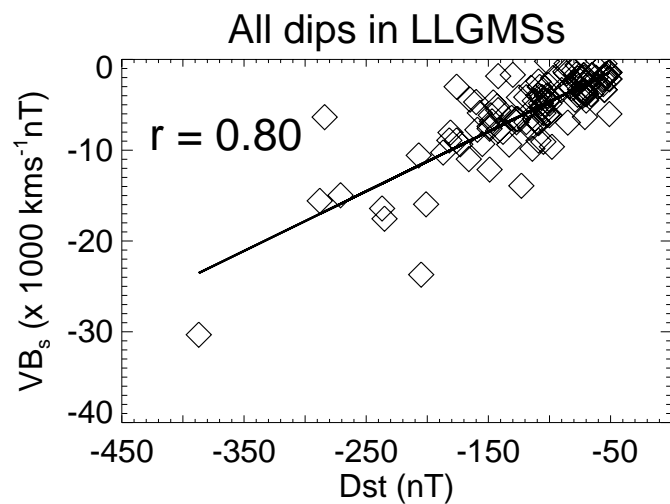
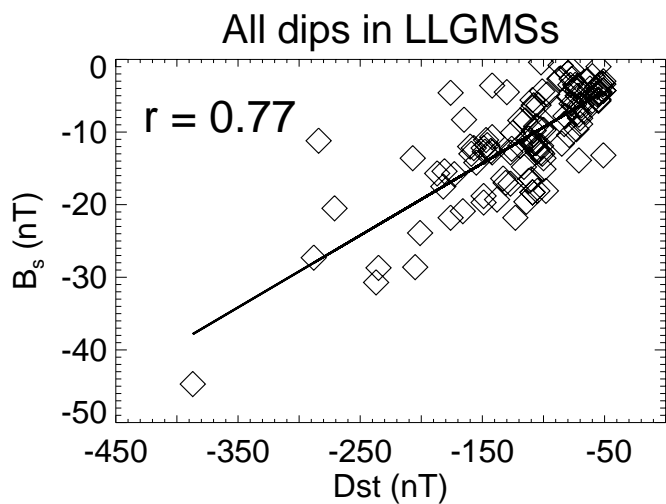


Table 1. Successive CME Association With Long Lived Geomagnetic Storms

Num	Dst_min Time ^a (UT)	Dst_min ^b (nT)	Start ^c (UT)	End ^d (UT)	Dur ^e (Day)	IP driver ^f	CME ^g	Source Loc. ⁱ	Category &Comments ^j
1998									
1	0218 01:00	-100	0217 12:00	0221 01:00	~3.5	MC + HSS	0214 06:55 (pH)	S24E23	S: (1, 1, h)
2	0307 00:00	-116	0310 11:00	0317 10:00	~8.1	HSS in CIR	-	-	C: (0, 0, h)
3	0504 06:00	-205	0502 02:00	0508 00:00	~5.9	Sh. + C. ICME	0429 16:58 (H) 0501 23:40 (H) 0502 05:31 (H) 0502 14:06 (H) 0503 22:02 (pH)	S18E20 S18W05 S20W07 S15W15 S13W34	M: (5, 3)
4	0806 12:00	-138	0806 00:00	0809 14:00	~3.6	MC + HSS	DG	-	S: (1, 1, h)
5	0827 10:00	-155	0826 09:00	0901 09:00	~6.0	Sh. + MCL+ HSS	DG	-	S: (1, 1, h)
6	0925 10:00	-207	0925 01:00	0929 13:00	~4.5	Sh. + MC + HSS	DG	-	S: (1, 1, h)
7	1019 16:00	-112	1019 00:00	10/23 14:00	~4.6	MC + HSS	10/15 10:04 (H) 11/05 02:02 (H)	N22W01 N19W10	S: (1, 0, h)
8	1108 07:00	-149	1108 21:00	1112 08:00	~3.5	C. ICME	11/05 20:44 (H) 11/06 02:18 (pH)	N22W18 N19W24	M: (3, 2)
9	1113 22:00	-131	1113 00:00	1117 12:00	~4.5	Sh. + 2 MCL + HSS	11/09 18:18 (pH) 11/10 06:18 (pH)	N18W02 N17W08	M: (2, 1, h)
1999									
10	0218 18:00	-123	0218 4:00	0221 14:00	~3.5	Sh. + C. ICME	DG	-	M: (3, 2)
11	1022 07:00	-237	1021 04:00	1029 19:00	~8.6	MCL + HSS	10/19 05:50 (pH)	S24E18	S: (1, 1, h)
12	1113 23:00	-106	1110 23:00	1115 21:00	~4.9	HSS + C. ICME	DG	-	M: (2, 0, h)
2000									
13	0212 12:00	-133	0211 04:00	0216 01:00	~4.9	C. ICME + Sh. + HSS	02/08 09:30 (H) 02/09 19:54 (H) 02/10 02:30 (H) 02/12 04:31 (H)	N25E26 S17W40 N31E04 N26W26	M: (4, 3, h)
14	0407 01:00	-288	0406 18:00	0412 12:00	~5.8	MCL + HSS	0404 16:32 (H)	N16W66	S: (1, 2, h)
15	0524 9:00	-147	0523 20:00	0526 22:00	~3.1	C. Sh. + ICME	0522 01:26 (H) 0520 14:50 (pH)	S20W48 S21W30	M: (2, 2)
16	0716 02:00	-301	0715 16:00	0718 20:00	~3.2	Sh. + MC	07/14 10:54 (H)	N22W07	S: (1, 2)
17	0812 10:00	-235	0810 3:00	0814 22:00	~4.8	2 MCs	08/09 16:30 (H) 08/06 18:30(pH) 0810 06:54 (pH)	N11W11 N10E30 N18E00	M: (3, 2)
18	0918 00:00	-201	0917 20:00	0921 22:00	~4.1	Sh. + 3 MCLs	09/15 21:50 (H) 09/16 05:18 (H) 0915 12:06 (pH) 0915 15:26 (pH)	N12E04 N14W07 N13E08 N12E07	M: (4, 2)
19	1005 14:00	-182	1002 07:00	1008 13:00	~6.3	Sh. + 4 MCLs	1002 03:50 (H) 1002 20:26 (H) 0929 21:50 (pH) 0930 18:06 (pH) 1001 13:50 (pH) 1003 08:06 (pH)	S09E07 S09E00 S11E13 S20E42 S10E15 N27W59	M: (6, 3)
20	1107 02:00	-159	1105 14:00	1108 11:00	~3.1	Sh. + 3 ICMEs (2 MCLs)	1103 18:26 (H) 11/02 16:26 (pH) 1104 01:50 (100)	N02W02 N23W58 S27 W30	M: (3, 2)
21	1129 14:00	-119	1126 16:00	1202 9:00	~5.4	Sh. + C. ICME	10 Halos	-	M: (10, 2)

2001									
22	0331 09:00	-387	0330 23:00	0403 21:00	~3.9	Sh. + MCL	03/28 01:27 (H.) 03/28 12:50 (H) 03/29 10:26 (H) 03/29 00:26 (106)	N20E22 N18E02 N20W19 N17W04	M: (4, 4)
23	1003 15:00	-166	0925 22:00	1005 14:00	~9.7	Sh. + HSS + C. ICME	0924 10:30 (H) 0928 08:54 (H) 0929 11:54 (H) 0928 10:30 (pH)	S16E23 N10E18 S13E03 S18W36	M: (4, 2, h)
24	1021 22:00	-187	1021 18:00	1025 10:00	~3.7	Sh. + C. ICME	1019 01:27 (H) 1019 16:50 (H) 1018 20:26 (pH)	N16W18 N15W29 S17E69	M: (3, 2)
25	1028 12:00	-157	1028 4:00	1031 14:00	~3.4	Sh. + C. ICME	1025 15:26 (H) 1026 20:50 (105)	S16W21 N09E08	M: (2, 0)
26	1106 07:00	-292	1105 19:00	1112 10:00	~6.6	Sh. + C. ICME +HSS	11/01 22:30 (H) 11/03 19:20 (H) 11/04 16:35 (H)	N12W23 N03W16 N06W18	M: (3, 3, h)
27	1124 17:00	-221	1124 07:00	1128 09:00	~4.1	Sh. + C. ICME (2 MCL)	1121 14:06 (H) 1122 20:30 (H) 1122 23:30 (H)	S14W19 S25W67 S17W24	M: (3, 3)
2002									
28	0420 09:00	-149	0417 12:00	0423 05:00	~5.7	Sh. + MC +HSS + MCL	0415 03:50 (H) 0417 08:26 (H)	S15W01 S14W34	M: (2, 1, h)
29	0523 18:00	-109	0522 02:00	0526 02:00	~4.0	C. Sh. + HSS	0522 03:50 (H) 0521 21:50 (pH) 0522 00:06 (pH)	S30W34 N17E38 S20W70	M: (3, 0, h)
30	0821 07:00	-106	0819 00:00	0822 19:00	~3.8	Sh. + C. ICME (2 MCs)	0816 12:30 (H) 0818 21:54 (pH) 0819 11:06 (pH) 0820 01:54 (pH)	S14E20 S08W28 S12W19 S11W35	M: (4, 0)
31	0904 06:00	-109	0903 20:00	0907 00:00	~3.2	HSS in CIR	-	-	C: (0, 0, h)
32	0908 01:00	-181	0907 01:00	0915 10:00	~10.4	Sh. + C. ICME + HSS	0905 16:54 (H) 0906 13:31 (H) 0904 13:31 (pH) 0908 15:06 (pH)	N09E28 N11W45 S15E07 N12E76	M: (4, 2, h) Pre. – 27 nT
33	1001 17:00	-176	0930 2:00	1003 10:00	~3.3	Sh. + MC	0928 01:31(89) 0928 11:06(79) 0929 08:06 (106)	N11E36 N12E33 S08W70	M: (3, 3)
34	1004 09:00	-146	1003 10:00	1006 15:00	~3.2	Sh. + 2 MCs	1002 07:31 (pH) 1003 03:54 (pH) 1003 05:54 (pH)	S18E20 S19E06 N13W29	M: (3, 0) Pre. – 45 nT
35	1007 08:00	-115	1006 15:00	1013 13:00	~6.9	HSS in CIR	-	-	C: (0, 0, h)
36	1014 14:00	-100	1013 13:00	1021 06:00	~7.7	HSS in CIR	-	-	C: (0, 0, h)
37	1121 11:00	-128	1121 3:00	1126 22:00	~5.8	HSS in CIR	-	-	C: (0, 0, h)

^aDst minimum time of the LLGMS.

^bDst minimum value of the LLGMS.

^cStart time of the LLGMS.

^dEnd time of the LLGMS.

^eDuration of the LLGMS.

^fInterplanetary driver causing southward IMFs. MCL = Magnetic Cloud Like, Sh. = Sheath, C. = Compressed or Compound

^gAssociated CME first appearance time in C2. Halo = Full Halo CME, pH = Partial Halo CME. If related CMEs are neither Halo or partial Halo, then their angular width are listed. DG = Data Gap.

^hThe apparent speed of the associated CMEs.

ⁱSolar source location of the associated CMEs.

³M = Multiple CME, S = Single CME, C = CIR. The 1st number in parentheses is the number of associated CMEs, 2nd number is the degree of interaction: the degree of 1 represents interaction between a CME and a HSS, otherwise, the degree is equal to the number of CMEs involved in the possible interaction, h = cases involving HSS events.